

Superconductivity and Fast Proton Transport in Nanoconfined Water

K. H. Johnson*

Department of Materials Science and Engineering

Massachusetts Institute of Technology, Cambridge, MA 02139

A real-space molecular-orbital description of Cooper pairing in conjunction with the dynamic Jahn-Teller mechanism for high- T_c superconductivity predicts that electron-doped water confined to the nanoscale environment of a carbon nanotube or biological macromolecule should superconduct below and exhibit fast proton transport above the transition temperature, $T_c \cong 230$ degK (-43 degC).

1. Introduction

A major goal of superconductor research and development is the discovery of useful substances that superconduct at the highest possible transition or critical temperatures, T_c . The Bardeen-Cooper-Schrieffer (BCS) theory of superconductivity,¹ which ascribes the onset of the superconducting state at the transition temperature T_c to electrons attractively paired via virtual phonons, has been eminently successful in explaining conventional, relatively low- T_c superconductors. However, BCS theory in its simplest form has failed to explain the origin of the high- T_c superconductivity of doped cuprates.² Coupled with the dynamic Jahn-Teller (DJT) effect³ and density-functional calculations for clusters representing the local molecular environments in superconducting materials,⁴ a *real-space molecular-orbital* description of electronic wave functions which are precursors of the superconducting state in high- and low-dimensional metals was proposed and applied to a variety of superconductors.⁵ According to this scenario, superconductivity is possible only if the normal chemical bonding system in the material or parts thereof permits the construction of vibronically-coupled degenerate or nearly-degenerate (“pseudo” Jahn-Teller) molecular-orbital wave functions at the Fermi energy (E_F) which, for at least one space direction, are not topologically intersected by plane or conical nodal surfaces.

*Professor Emeritus; kjohnson@mit.edu

This translates to the requirement of spatially delocalized molecular orbitals at E_F that are bonding along “channels” of opposite phase, Ψ_+ and Ψ_- which are a *coordinate-space* basis for the *Cooper-pair wavefunction*,

$$\Phi(\mathbf{r}) = \langle \Psi_+(\mathbf{r}+\mathbf{d}/2)\uparrow \Psi_-(\mathbf{r}-\mathbf{d}/2)\downarrow \rangle, \quad (1)$$

where \mathbf{r} is the pair spatial vector and \mathbf{d} is the distance between the Ψ_+ and Ψ_- “channels,” beyond which the electron-electron repulsion at E_F is largely screened out by the intervening ion cores (see Figs. 2, 4, and 5).⁵ The theory was applied to conventional metallic and organic superconductors,^{5,6} high- T_c cuprates,⁶ and superconducting potassium-doped carbon fullerene,⁷ yielding T_c -values, coherence lengths, isotope shifts, Debye frequencies, and thermodynamic critical magnetic fields in good agreement with experiments. Major findings include the association of cuprate high- T_c superconductivity with DJT vibronically-coupled, mainly oxygen orbitals at E_F , the prediction of 230 degK (-43degC) as the upper limit of T_c , and reduction of the theory to conventional BCS theory in the limit of harmonic vibronic (electron-phonon) coupling.^{5,6} In the present paper, we propose that *supercooled, nanoscopically confined, electron-doped* water should superconduct up to the highest predicted $T_c \cong 230$ degK due to DJT-induced terahertz (THz) vibrations of the component water nanoclusters coupled with their degenerate, mainly oxygen molecular orbitals at E_F . Above $T_c \cong 230$ degK, nanoconfined water should exhibit high proton conductivity.

2. Review of the Theory Applied to High- T_c Cuprates and Fullerenes

Common to all the high- T_c cuprates is the approximately square-planar CuO_4 coordination complex forming the CuO_2 layers. Key to understanding both the parent insulating and superconducting phases of the cuprates is the strong covalency between the copper 3d atomic orbitals and the oxygen 2p valence orbitals, as compared with transition metals and oxygen. As a result, the relative ordering and characters of the $\text{Cu}(d)$ - $\text{O}(p)$ σ and π molecular-orbital levels in a CuO_4 coordination complex, determined from density-functional theory and shown in Fig. 1(b) are significantly different from those of the ligand-field levels for a typical ionic transition-metal complex ML_4 shown in Fig. 1(a). This is due to the strong $\text{Cu}(d_{xz,yz}\pi^*)$ - $\text{O}(p_z\pi)$ covalent *antibonding* hybridization. It may be noted that some previous theories of high- T_c superconductivity have assumed that the ordering of electron states in the doped CuO_4 complexes of the CuO_2 layers is the same as the ML_4 ligand-field levels of Fig. 1(a). That is simply incorrect. Occupancy of the strongly

localized σ^* -antibonding b_{1g} $\text{Cu}(d_{x^2-y^2})\text{-O}(p_{x,y})$ orbital shown schematically in Fig. 1(b) is associated with the non-superconducting state of *undoped* cuprates. *Hole doping* leads to partial occupancy of the doubly degenerate e_g $\text{O}(p_z)\text{-Cu}(d_{xz,yz})$ π^* -antibonding molecular orbital shown schematically in Fig. 1(b) and in the density-functional $e_g(xz)$ wavefunction contour map of Fig. 2. Note the predominant $\text{O}(p_z\pi)$ character. These coordinate-space e_g orbitals correspond to the \mathbf{k} -space *flat-band 4 and Van Hove singularity* at E_F above the mainly oxygen-like valence band shown in the reproduced Fig 3(a).⁸ The real-space $e_g(xz)$ molecular-orbital wavefunction contour map of Fig. 2 is very similar topologically to the charge-density map shown in Fig. 3(b) for this flat-band Van Hove singularity.⁸ The key consequence of this strong $\text{O}(p_z)\text{-Cu}(d_{xz,yz})$ π^* -antibonding hybridization at E_F for optimally doped high- T_c cuprates (not pointed out previously in publications by other authors) is the promotion of substantial $\text{O}(p_z\pi)\text{-O}(p_z\pi)$ bond overlaps of opposite phase, Ψ_+ and Ψ_- *above and parallel to the CuO_2 layers*, as revealed in the contour map of the $e_g(xy)$ molecular-orbital wavefunction plotted 0.8 Å above the CuO_2 layer in Fig. 2. The occupancy and $\text{O}(p_z\pi)\text{-O}(p_z\pi)$ bond overlaps within the Ψ_+ and Ψ_- channels depend sensitively on the doping and further details of the electronic structure, such as the “puckering” of the CuO_2 layers and their CuO_4 coordination complexes, the presence of apical oxygens above and below the CuO_2 layer in $\text{La}_{2-x}\text{Sr}_x\text{CuO}_4$, and the presence of chains above and below the CuO_2 layers in $\text{YBa}_2\text{Cu}_3\text{O}_7$. The key point here is that *common to all* the optimally doped HTSC cuprates at E_F , there is significant $\text{O}(p_z\pi)\text{-O}(p_z\pi)$ bond overlap (equivalent to oxygen-oxygen hole “hopping”) *above and parallel to* (but *not within*) the CuO_2 layers, forming the basis, Ψ_+ and Ψ_- of a *Cooper-pair “density wave” above and parallel to each CuO_2 layer* in coordinate space as shown schematically in Fig. 4. A Cooper-pair density wave has indeed recently been detected in the cuprate, $\text{Bi}_2\text{Sr}_2\text{CaCu}_2\text{O}_{8+x}$.⁹

In the example of potassium-doped fullerene, icosahedral (I_h -symmetry) C_{60} “buckyballs” are arranged in an fcc structure such that the electronic states at E_F in real space are derived from degenerate $t_{1u}(p\pi)$ molecular orbitals that are bonding around the hemisphere of each buckyball and overlap, forming the *Cooper-pair basis wavefunctions*, Ψ_+ and Ψ_- shown along one of three equivalent directions in Fig 5.⁷ The interstitial K^+ ions that donate their valence electrons into the normally unoccupied buckyball $t_{1u}(p\pi)$ molecular orbitals are not shown. Because of the C_{60} $t_{1u}(p\pi)$ molecular-orbital degeneracy and partial occupancy at modest potassium electron doping, each buckyball is subject to the DJT effect,³ as is well known to occur in other $p\pi$ aromatic systems such as the benzene molecular ion.¹⁰ Due to the modest overlaps of the C_{60} $p\pi$ orbitals within the

Ψ_+ and Ψ_- channels, the DJT I_h -symmetry-breaking vibrations (H_g modes) of the buckyballs occur *coherently* and correspond to “soft-phonon” modes in the solid K_xC_{60} .

Based on the above molecular-orbital Ψ_+ and Ψ_- topologies in both the doped cuprates and fullerenes, the Cooper pair can then be described as the *coordinate-space wavefunction*, Eq. 1. Including the symmetry-breaking effect of DJT vibronic (*local* electron-phonon) coupling of the degenerate Ψ_+ and Ψ_- electronic states and solving the Schrödinger wave equation approximately for the Cooper-pair wavefunction, Eq.1 yields the following general practical formula for T_c ,^{5,6}

$$k_B T_c \cong h\nu_c \exp\{-h^2/2me^2d[1-(m/M)^\beta]\}, \quad (2)$$

and DJT vibrational cut-off frequency,

$$\nu_c \cong h(m/M)^\beta/4\pi md^2, \quad (3)$$

where k_B is the Boltzmann constant, m is the electron mass, and M is the mass of the DJT-vibrating atom (oxygen mass number $M = 16$ in the cuprates and carbon mass number $M = 12$ in fullerene), The DJT vibronic coupling parameter, β is determined from the respective computed O-O and C_{60} - C_{60} $p\pi$ -bond overlaps within the Ψ_+ and Ψ_- channels (see Fig. 7a).⁵⁻⁷ For the “*harmonic limit*,” $\beta = 1/2$, formula (2) is the real-space equivalent of BCS theory, and ν_c reduces to the Debye frequency.⁵⁻⁷ For $1/4 < \beta < 1/2$, the DJT effect corresponds to *anharmonic electron-phonon coupling*, moving ν_c into the terahertz (THz) range. For $\beta < 1/4$, there is the possibility of reaching the highest T_c of 230 degK (curve “e” of Fig. 6a), although the *static Jahn-Teller effect* can compete with the DJT effect and make the system structurally unstable, preventing Cooper pairing.^{3,5} Indeed, the highest- T_c materials have tended to lose their superconductivity because of structural changes induced by the static Jahn-Teller effect. Formulae (2) and (3) were applied to the high- T_c cuprates⁶ and potassium-doped fullerene,⁷ yielding results in excellent agreement with experiments. Graphs of T_c and isotope effect, $\alpha = -\partial \ln T_c / \partial \ln M$ versus β for oxygen mass number $M = 16$ and various values of the Ψ_+ - Ψ_- interchannel distance, d displayed in Fig. 6 are representative of both the cuprates *and* of confined water (see Section 4), where oxygen is the DJT vibronically active element responsible for superconductivity. Note the vanishing of the isotope effect at the T_c curve peaks in Fig. 6b. The relationship between anharmonicity, β and $O(p\pi)$ - $O(p\pi)$ bond overlap within the Ψ_+ and Ψ_- channels (Figs. 2 and 4) is shown in Fig. 7a. All high- T_c cuprates lie between curves b and c of Fig. 6, and the upper limit of $T_c \cong 230$ degK

is predicted for oxides with $\Psi_+ - \Psi_-$ interchannel distance, $d \cong 8 \text{ \AA}$. The present DJT mechanism sets an upper limit of $T_c \cong 230 \text{ degK}$ (-43 degC) for *any* potential superconductive material, as exemplified for hydrogen in Fig. 7b. T_c graphs for K_xC_{60} are similar. A report of sporadic superconductivity at $T_c = 230 \text{ degK}$ in one sample of the cuprate, $\text{EuBa}_2\text{Cu}_3\text{O}_{6+\delta}$ was published years ago.¹¹ Recently, hydrogen sulfide at high pressure has been observed to superconduct at $T_c = 203 \text{ degK}$ by an attributed anharmonic electron-phonon mechanism,¹² which could possibly be the DJT mechanism presented here.

3. Predicted Superconductivity of Nanoconfined Water Below $T_c \cong 230 \text{ degK}$

In Fig.5, one can view fcc superconducting K_xC_{60} ($x = 3$) as a system of “confined” $(C_{60})^{-3}$ buckyball clusters stabilized by the surrounding interstitial potassium ions K^+ , which have donated one electron per K^+ ion into the otherwise lowest unoccupied, six-fold degenerate $t_{1u}(p\pi)$ molecular orbital (LUMO) of each C_{60} cluster, subject to DJT vibronic (anharmonic electron-phonon) coupling. This observation and the recent experimental evidence for high- T_c superconductivity in hydrogen sulfide (H_2S) at high pressure by an anharmonic electron-phonon mechanism¹² leads one to consider nanoconfined water (H_2O) as a possible superconductor. However, the limitation of $T_c \cong 230 \text{ degK}$ by the present theory would suggest only *supercooled* nanoconfined water as a possibility. Water can be rapidly supercooled to -43 degC (230 degK) – the upper limit to superconducting T_c according to the present theory – or lower by confining water at nanoscale, *e.g.* in nanotubes.¹³ Recent x-ray studies of water supercooled to -15 degC in a quartz capillary have revealed the presence of pentagonal dodecahedral and other pentagonal water clathrate nanoclusters similar to those shown in Figs. 8 and 10, which become dominant with decreasing temperature.¹⁴ Therefore, it is expected that this trend would continue at even lower temperatures in a nanoscale environment. Pentagonal water clusters have been shown to be present in nanotubes¹³ and proteins near hydrophobic amino acids,¹⁵ where the hydrophobicity promotes the pentagonal clustering of water molecules. THz vibrations of water nanoclusters have been argued to be key to biomolecular function such as protein folding.¹⁶

Fig. 8 shows the computed density-functional ground-state molecular-orbital energies and vibrational modes of the *protonated* pentagonal dodecahedral water cluster, $(\text{H}_2\text{O})_{21}\text{H}^+$ or $(\text{H}_2\text{O})_{20}\text{H}_3\text{O}^+$. Like icosahedral C_{60} buckyballs, pentagonal dodecahedral water clusters have their oxygens at the vertices of a dodecahedron having I_h icosahedral symmetry. Of particular

importance are the “squashing” and “twisting” vibrational modes of a pentagonal dodecahedral cluster shown in Fig. 9. Density-functional calculations for the pentagonal dodecahedral water cluster, $(\text{H}_2\text{O})_{20}$, and larger water clusters yield the vibrational modes in Fig. 10. Common to all the water nanoclusters studied are: (1) lowest unoccupied (LUMO) energy levels like those in Fig. 8a, which correspond to the “S”-, “P”-, “D”- and “F”-like cluster “surface” orbital wavefunctions in Fig. 8b; and (2) bands of vibrational modes between 1 and 6 THz (Figs. 8 and 10) due to O-O-O “squashing” (or “bending”) and “twisting” motions of the type in Fig. 9. The vectors in Figs. 8 and 10 represent the directions and relative amplitudes for the lowest THz modes corresponding to the O-O-O “bending” (or “squashing”) motions of the water-cluster “surface” oxygen ions. Surface O-O-O bending vibrations of water clusters in this THz range have been observed experimentally.¹⁷ When an extra electron is transferred to the LUMOs - the so-called *hydrated electron* - it is a bound state.¹⁸ Thus, *electron doping* can put electrons into stable water-cluster molecular orbitals - *e.g.* the $p\pi$ orbitals of Figs. 8b and 11 - that are precursors to forming the Ψ_+ and Ψ_- *coordinate-space Cooper-pair wavefunction*, Eq. 1, as exemplified in Figs. 4 and 5 respectively for a hole-doped cuprate and electron-doped fullerene. Moreover, like the cuprate high- T_c scenario above (Figs. 2 and 4), it is the overlapping *oxygen* $p\pi$ orbitals surrounding the water nanocluster surfaces (Figs. 8b and 11) that should Cooper-pair (Eq. 1) via the DJT effect below $T_c \cong 230$ degK, provided the electron-doped, hydrated-electron water clusters are aggregated and supercooled to the solid state.

To accomplish this, one can confine water to *nanoscopic* environments such as carbon nanotubes,¹³ silica capillaries,¹⁴ or proteins,^{15,16} where water can form nanoclusters responsible for the observed anomalously soft dynamics and anomalous quantum state of protons in nanoconfined water, including evidence for *anharmonic* intermolecular potentials and large-amplitude motions in nanotube water.^{19,20} In the hydrophobic environment of a simple single-wall nanotube, water molecules can bond together to form clusters like the ones in Figs. 8-11, as shown in Fig. 12. Density-functional electronic-structure calculations for *electron-doped* water clusters of diameter 8 Å (0.8 nm) confined to a 12 Å (1.2 nm) single-wall carbon nanotube have been performed and yield overlapping hydrated-electron water-cluster “surface” $p\pi$ molecular orbitals for neighboring confined water clusters like those shown in Figs. 12 and 13. The latter are the basis, Ψ_+ and Ψ_- , for *coordinate-space Cooper pairing* in Eq. 1 via DJT vibronic coupling with the water-cluster oxygen surface THz-frequency vibrational modes like the ones shown by the vector

amplitudes in Figs. 8 and 10, although there is also weak coupling of the water-cluster modes to THz vibrations of the nanotube walls.

While signs of superconductivity at only 0.55 degK in “ropes” of (presumably) “dry” carbon nanotubes have been observed,²¹ there has been a recent claim of high- T_c superconductivity in *water-treated graphite* powder.²² The above formula (2) applied to nanotube-confined water clusters of diameter $d = 8 \text{ \AA}$ (0.8 nm) for a DJT coupling constant $\beta = 0.11$ – determined from the water-cluster $O(p\pi)-O(p\pi)$ bond overlap (Figs. 7a and 13b)^{5,6} – predicts a maximum $T_c \cong 230 \text{ degK}$, like that for the cuprates (Fig. 6a, curve “e”) – a very high T_c , but indicating *no possibility* of “room-temperature” superconductivity. Again, it must be emphasized that this prediction of superconductivity in nanotube-confined water depends on the effective *electron doping* of the water, which can be done in the laboratory is several ways.

4. Fast Proton Transport in Carbon-Nanotube-Confined Water Above $T_c \cong 230 \text{ degK}$

If nanotube-confined water clusters are *protonated*, like the ubiquitous $(H_2O)_{21}H^+$ cluster shown in Fig. 8, and then electron-doped, *i.e.* electrons are added to the LUMOs, occupation of the LUMO cluster molecular orbitals shown in Figs. 8a and 8b will induce the symmetry-breaking dynamical Jahn-Teller effect (Fig. 9), which causes each confined water nanocluster (Fig. 13a,b) to oscillate *anharmonically* between “double-well potentials” (Fig. 13c) along the nanotube, lowering the energy barrier, E_{barrier} for proton tunneling between neighboring water clusters. This is consistent with the observed anomalously soft dynamics and anomalous quantum state of protons in nanoconfined water, including evidence for *anharmonic* intermolecular potentials and large-amplitude motions in nanotube-confined water.^{19,20} This promotes fast transport of protons through nanotube-confined water, as recently observed experimentally in sub-1-nm diameter carbon nanotube porins.²³ The phase-change transition temperature from superconducting Cooper pairs, Eq. 1, to highly conducting protons is given by Eq. 2 (the same T_c formula for the upper limit of electronic superconductivity) because that phase change can be viewed as a transition from the *dynamic* to *cooperative* Jahn-Teller effect.³ For confined 0.8-nm-diameter water nanoclusters like those shown in Fig. 12, $T_c \cong 230 \text{ degK}$. Using Eq. 2, $\nu_c \cong 29 \text{ THz}$, which is close to the upper-frequency limits shown in Figs. 8c and 10 for isolated water-cluster O-H “librational modes” which should promote proton transport *above* $T_c \cong 230 \text{ degK}$, whereas *below* T_c , the watercluster mainly oxygen “surface vibrations” should promote superconductivity.

5. Fast Proton Transport in Biologically-Confined Water Above $T_c \cong 230$ degK

Another example of nanoconfined water is hydrated *phycocyanin*, the active center of an important light-harvesting protein,²⁴ where high electrical conduction possibly due to fast proton hopping has been experimentally observed to occur from -40 degC to room temperature, in good agreement with the above predicted T_c value, -43 degC (230 degK) for fast proton transport.²⁵ First-principles molecular-dynamics calculations and experiment²⁵ reveal the formation of water nanoclusters within the phycocyanin cavities as shown in Fig. 14a. Density-functional calculations indicate the presence of degenerate water-cluster “ $p\pi$ ” molecular orbitals like the ones shown in Fig. 14b and Fig. 11 that are subject to the cooperative JT effect and its promotion of proton transport as described above. It is also possible that *below* $T_c \cong 230$ degK, these orbitals form the basis, Ψ_+ and Ψ_- for coordinate-space Cooper pairing and therefore possible superconductivity of biologically-confined water as predicted above for nanotube-confined water.

6. Summary and Conclusions

Almost thirty years since the discovery of the high- T_c cuprates there is still no consensus on the origin of its unusual superconductivity beyond associating it principally with the oxygen ions. Although “non-phonon” mechanisms for the cuprates have been popular over the years, the present, universal “*real-space*” theoretical model for superconductors, first proposed over thirty years ago⁵ and applied with some success to the cuprate and fullerene superconductors,^{6,7} is most consistent with “*k-space*” electron-phonon mechanisms for the cuprates based on van Hove singularities in the flat, mainly oxygen band at E_F .^{8,26,27} (see Fig. 3a). The recent observation of a “*real-space*” Cooper-pair density wave in $\text{Bi}_2\text{Sr}_2\text{CaCu}_2\text{O}_{8+x}$ may add some credibility to the present DJT *real-space* molecular-orbital scenario.⁹ Adapting this scenario to nanoconfined water, it is predicted that DJT-induced “water-nanocluster surface” (mainly oxygen) vibrations (anharmonic local phonons) in the 1-6 THz range (Figs. 8 and 10) should promote *hydrated-electron* Cooper pairing and superconductivity of the nanoconfined water below $T_c \cong 230$ degK, whereas above this T_c , the confined water-nanocluster “librational” modes (mainly hydrogen librations) in the 10-32 THz range (Figs. 8 and 10) should dominate and promote fast proton conduction. While there is indeed recent experimental evidence for fast proton transport in nanotubes²³ and the protein, *phycocyanin*,²⁵ it remains to be proven that such nanoconfined water will also electronically superconduct below $T_c \cong 230$ degK, as predicted in this paper.

7. Acknowledgements

The author thanks M. Price-Gallagher, Y. Feldman, and Y. Paltiel for helpful discussions.

References

1. J. Bardeen, L. N. Cooper, and J. R. Schrieffer, Phys. Rev. **108**, 1175 (1957).
2. J. G. Bednorz and K. A. Muller, Z. Phys. B **64**, 189 (1986).
3. I. B. Bersuker and V. Z. Polinger, *Vibronic Interactions in Molecules and Crystals* (Springer- Verlag, New York, 1990).
4. J. C. Slater and K. H. Johnson, Phys. Rev. B **5**, 844 (1972).
5. K. H. Johnson and R. P. Messmer, Synthetic Metals **5**, 151 (1983).
6. K.H. Johnson et al., *Novel Superconductivity* (Plenum, New York, 1987) p.563; Physica C **153-155**, 1165 (1988); D.P. Clougherty and K.H. Johnson, Physica C **153-155**, 699 (1988); D.P. Clougherty, K.H. Johnson and M.E. McHenry, Physica C **162-164**, 1475 (1988); K.H. Johnson, D.P. Clougherty, and M.E. McHenry, in *Electronic Structure and Mechanisms for High- T_c Superconductivity*, eds. J. Ashkenazi and G. Vezzoli (Plenum, New York, 1991).
7. K.H. Johnson, M.E. McHenry and D.P. Clougherty, Physica C **183**, 319 (1991).
8. J. Yu, S. Massidda, and A. J. Freeman, Phys. Lett. A **122**, 203 (1987).
9. M.H. Hamidian et al., Nature **532**, 343 (2016).
10. L. Salem, *The Molecular Orbital Theory of Conjugated Systems* (Benjamin, New York, 1966) p. 466.
11. C. Y. Huang et al., Nature **328**, 403 (1987).
12. A.P. Drozdov et al., Nature **525**, 73 (2015).
13. P.M.G.L. Ferreira et al., Phys. Chem. Chem. Phys. **17**, 32126 (2015).
14. H. Yokoyama, M. Kannami and H. Kanno, Chem. Phys. Lett. **463**, 99 (2008).
15. M.M. Teeter, Proc. Natl. Acad. Sci. **81**, 6014 (1984).

16. K.H. Johnson, J. Biol. Phys. **38**, 85 (2012).
17. J. Brudermann, P. Lohbrandt and U. Buck, Phys. Rev. Lett. **80**, 2821 (1998).
18. K. Jordan and M.A. Johnson, Science **329**, 42 (2010).
19. A.I. Kolesnikov et al., Phys. Rev. Lett. **93**, 035503-1 (2004).
20. G.F. Reiter et al., Phys. Rev. B **85**, 045403 (2012).
21. M. Kociak et al., Phys. Rev. Lett. **86**, 2416 (2001).
22. T. Scheike et al., Adv. Mater. **24**, 5826 (2012).
23. R.H. Tunuguntla et al., Nature Nanotechnology **11**, 639 (2016).
24. A.N. Glazer, J. Biol. Chem. **264**, 1 (1989).
25. Y. Feldman and Y. Paltiel, manuscript in preparation.
26. J. Bouvier and J. Bok, Adv. Cond. Matt. Phys. **2010**, 1 (2010).
27. A. Piriou et al., Nature Comm. 1 Mar 2011, 1.

Figure Captions

Fig. 1. (a) Ligand-field electron states of a typical square-planar transition-metal complex, ML_4 . (b) Molecular-orbitals of a square-planar CuO_4 cluster.

Fig. 2. Wavefunction contour maps of the CuO_4 cluster $e_g(xy)$ and $e_g(xz)$ molecular-orbitals.

Fig. 3. (a) Fig. 1 of Ref. 8. $YBa_2Ba_2Cu_3O_7$ energy bands near E_F . (b) Fig. 5 of Ref 8. Charge-density counter map for band 4 of (a). Compare with $e_g(xz)$ molecular orbital in Fig. 2.

Fig. 4. The degenerate, coordinate-space, molecular-orbital basis, Ψ_+ and Ψ_- of the Cooper-pair wavefunction, Eq. 1 above and parallel to each CuO_2 layer of a typical high- T_c cuprate superconductor.

Fig. 5. The coordinate-space basis, Ψ_+ and Ψ_- of the Cooper-pair density wave for a potassium-doped fullerene superconductor.

Fig. 6. Graphs of superconducting transition temperature, T_c and isotope effect, α versus dynamic Jahn-Teller coupling parameter, β for oxygen mass number $M = 16$ and various values of Cooper-pair $\Psi_+ - \Psi_-$ interchannel distance d according to Eq. (2).

Fig. 7. a. Graph showing the relationship of $O(p\pi)-O(p\pi)$ bond overlap within the Cooper-pair basis Ψ_+ and Ψ_- channels and the DJT coupling parameter, β . **b.** Graph of superconducting transition temperature, T_c versus dynamic Jahn-Teller coupling parameter, β for hydrogen and various values of the Cooper-pair $\Psi_+ - \Psi_-$ interchannel distance, d according to Eq. (2).

Fig. 8. Ground-state density-functional molecular-orbital states and vibrational modes of an $(H_2O)_{21}H^+$ protonated pentagonal dodecahedral water nanocluster. **a.** Cluster molecular-orbital energy levels. **b.** Wavefunctions of the lowest unoccupied cluster molecular orbitals. **c.** Vibrational spectrum. **d.** The 1.5 THz vibrational mode. The vectors show the directions and relative amplitudes of the O-O-O “bending” oscillations of the cluster “surface” oxygen atoms.

Fig. 9. “Squashing” and “twisting” vibrational modes of a pentagonal dodecahedron. Hg and Hu designate the key irreducible representations of the icosahedral point group corresponding to these modes.

Fig. 10. a. Vibrational spectrum of a pentagonal dodecahedral $(\text{H}_2\text{O})_{20}$ water cluster. **b.** Lowest-frequency THz vibrational mode of the cluster. **c.** Vibrational spectrum of an array of three dodecahedral water clusters. **d.** Lowest-frequency THz vibrational mode. **e.** Vibrational spectrum of an array of five dodecahedral water clusters. **f.** Lowest-frequency THz vibrational mode. The vectors show the directions and relative amplitudes for the O-O-O “bending” motions responsible for the “squashing” mode of the cluster “surface” oxygen atoms.

Fig. 11. Hydrated-electron “ $p\pi$ ” molecular-orbital wavefunction of a water nanocluster consisting of three connected pentagonal dodecahedra. See Fig. 3c,d for THz vibrations thereof.

Fig. 12. (a) Hydrated-electron “ $p\pi$ ” molecular-orbital wavefunction of a water nanocluster of diameter 0.8 nm (8 Å) confined to a single-wall 1.2-nm-diameter carbon nanotube saturated at its ends with hydrogen. **(b)** Hydrated-electron “ $p\pi$ ” molecular-orbital wavefunction of a water nanocluster of diameter 0.8 nm confined to a single-wall 1.2-nm-diameter carbon nanotube.

Fig. 13. (a) Hydrated-electron “ $p\pi$ ” molecular-orbital wavefunctions of pentagonal dodecahedral water clusters of diameter 0.8 nm confined to an array of 1.2-nm-diameter single-wall carbon nanotubes (displayed end-on) labeled with the Ψ_+ and Ψ_- components of the Cooper-pair wavefunction. **(b)** Overlapping hydrated-electron “ $p\pi$ ” molecular-orbital wavefunctions of nanoconfined neighboring pentagonal dodecahedral water clusters labeled with the Ψ_+ and Ψ_- components of the Cooper-pair wavefunction. **(c)** Double potential energy wells for Jahn-Teller distorted water pentagonal dodecahedral water clusters (Fig. 9) and the resulting reduction of the energy barrier to proton transport between nanotube-confined neighboring water nanoclusters.

Fig 14. (a) Structure of the light-harvesting protein, phycocyanin confining a water nanocluster. **(b)** Hydrated-electron “ $p\pi$ ” molecular-orbital wavefunction of the phycocyanin-confined water nanocluster.

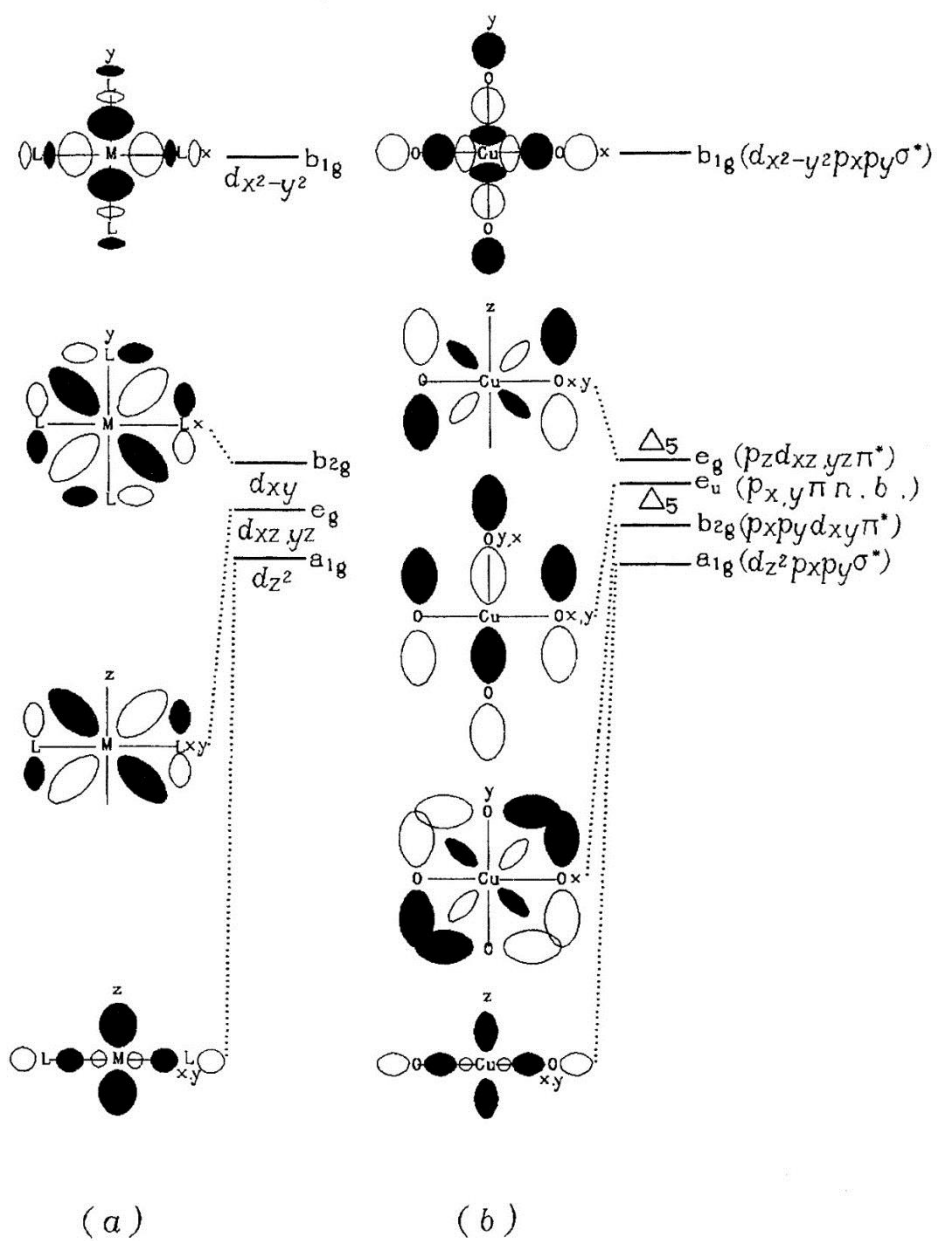


Fig. 1

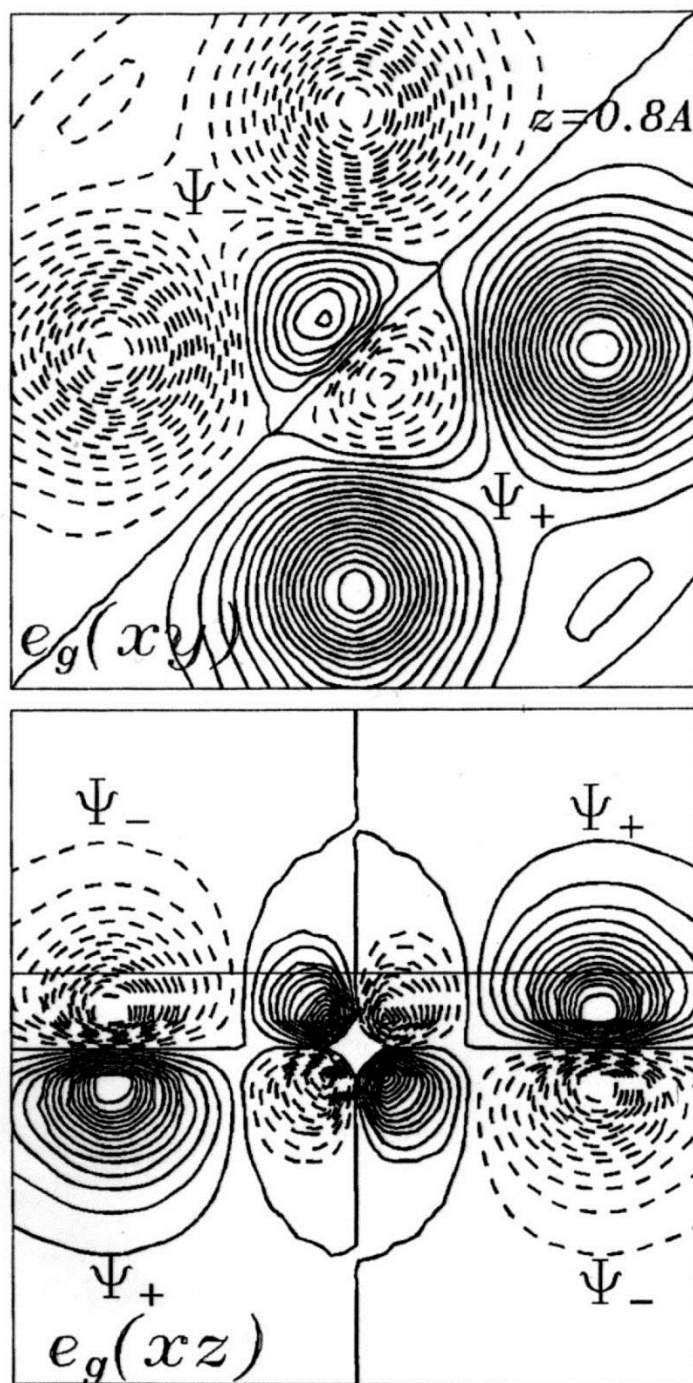
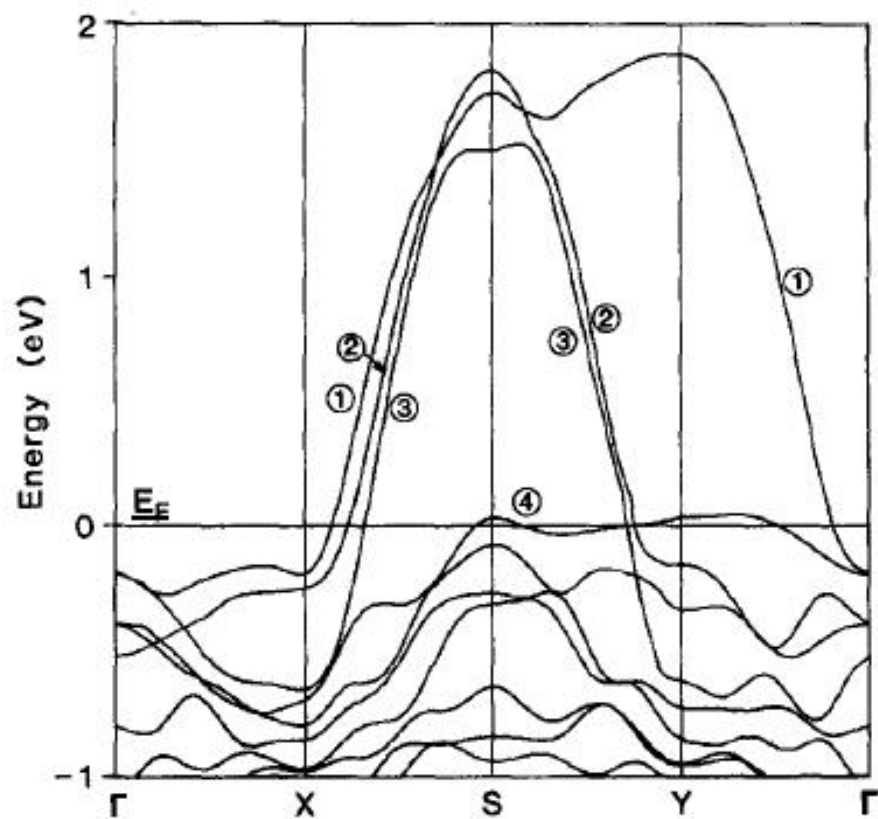
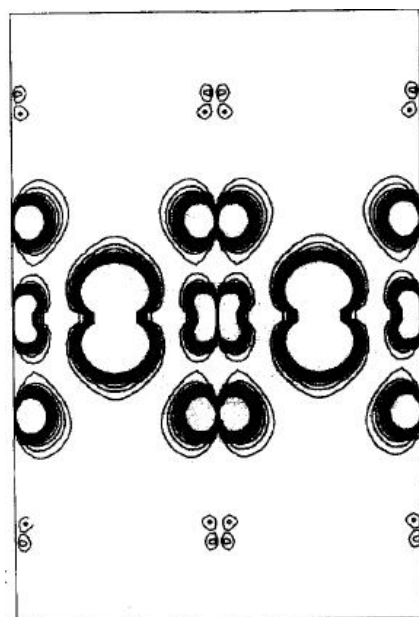


Fig. 2



(a)



(b)

Fig. 3

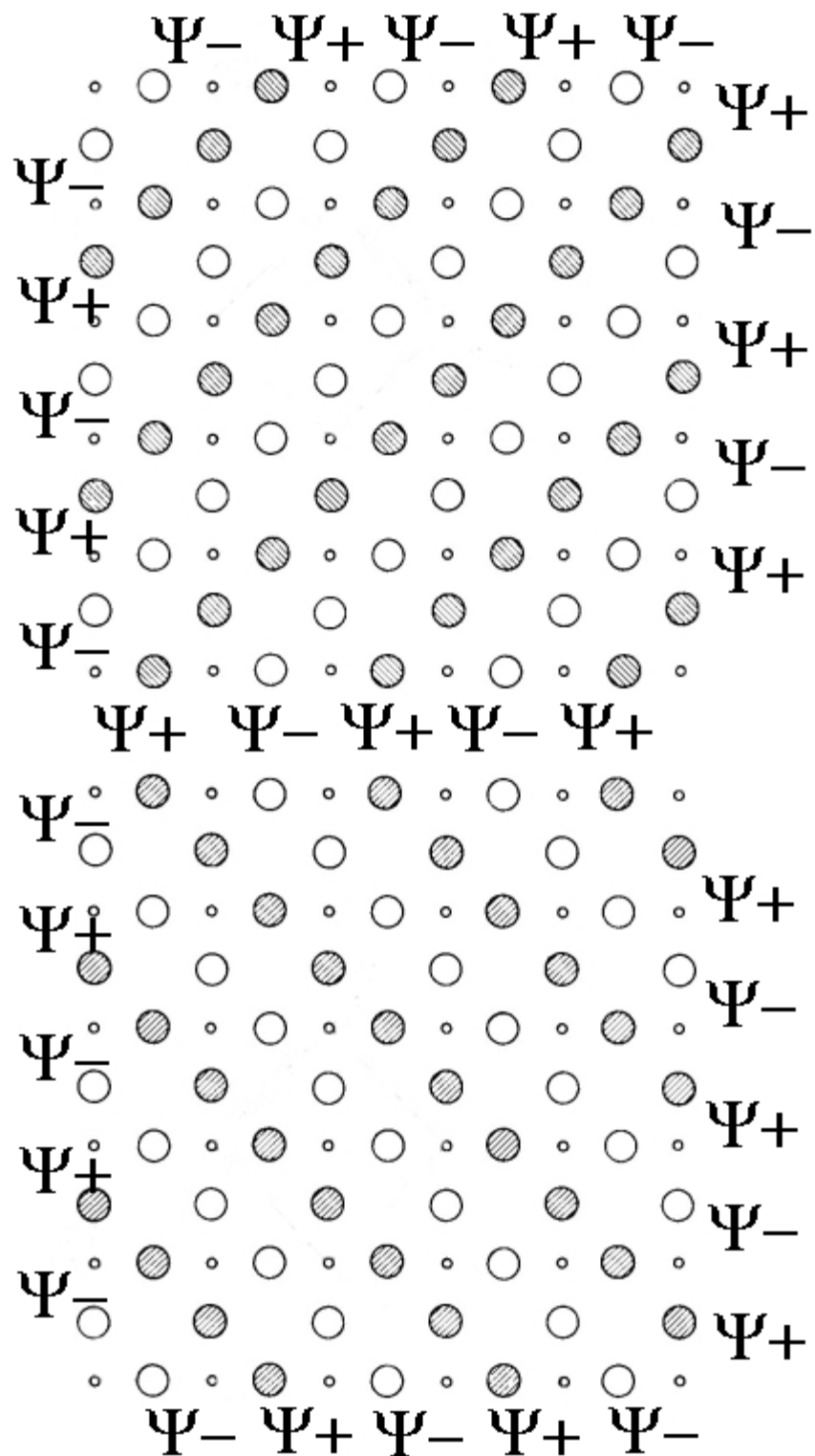


Fig. 4

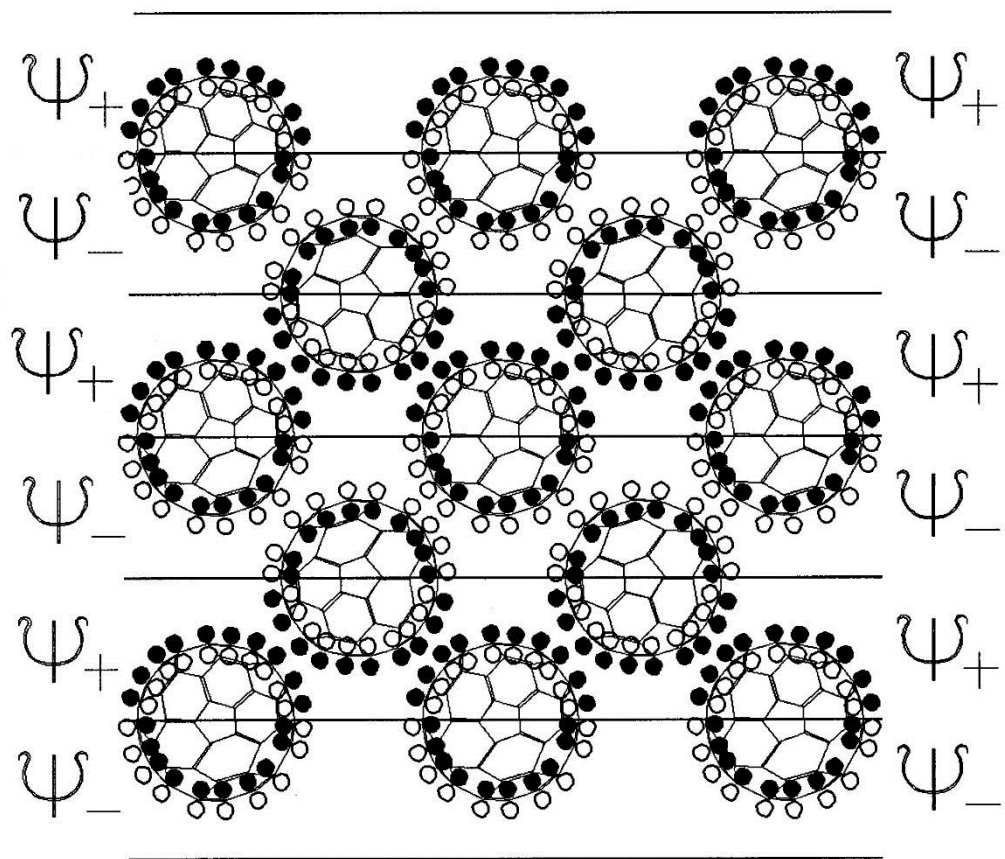


Fig. 5

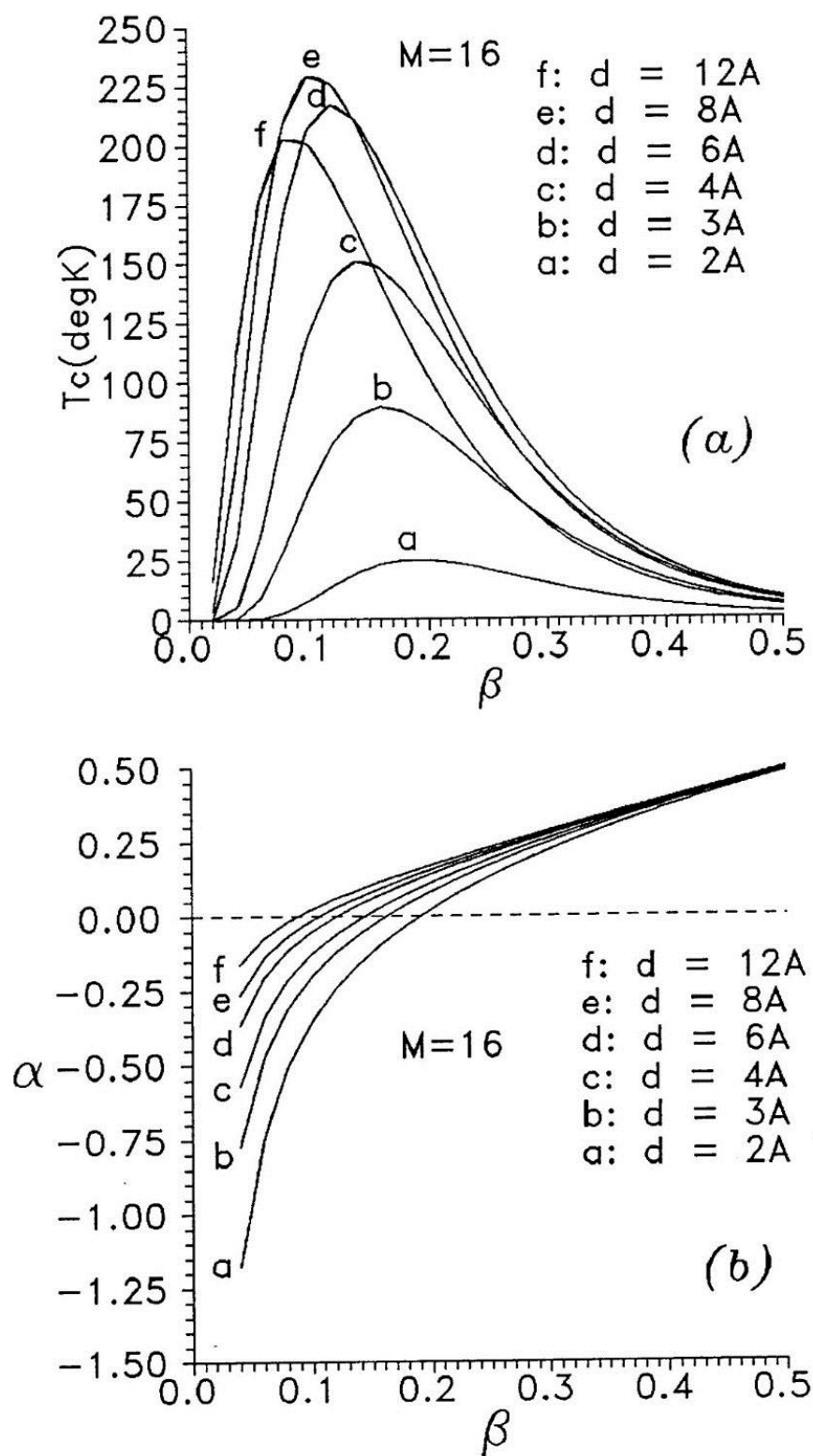
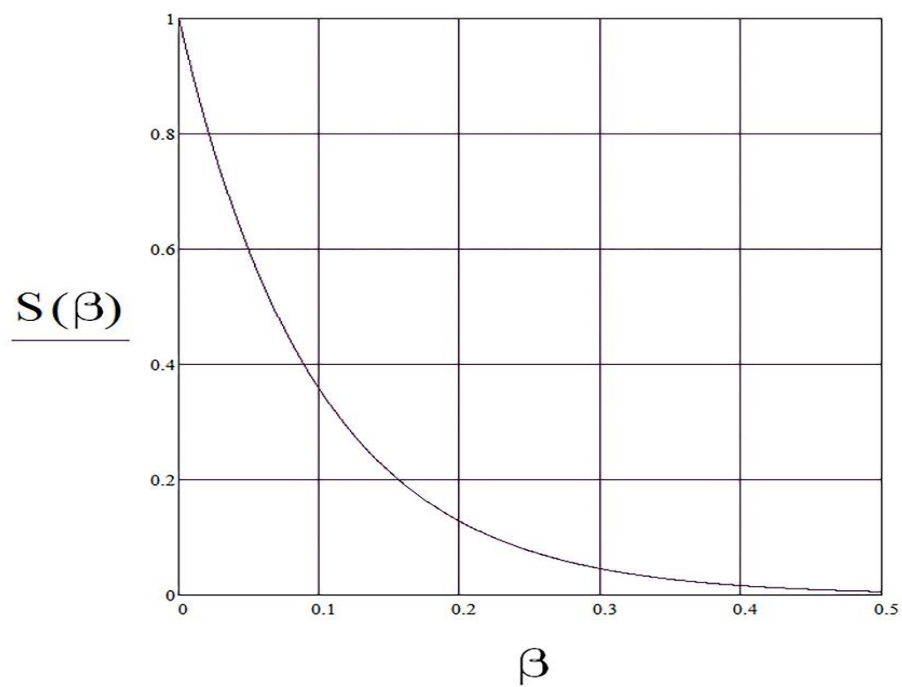
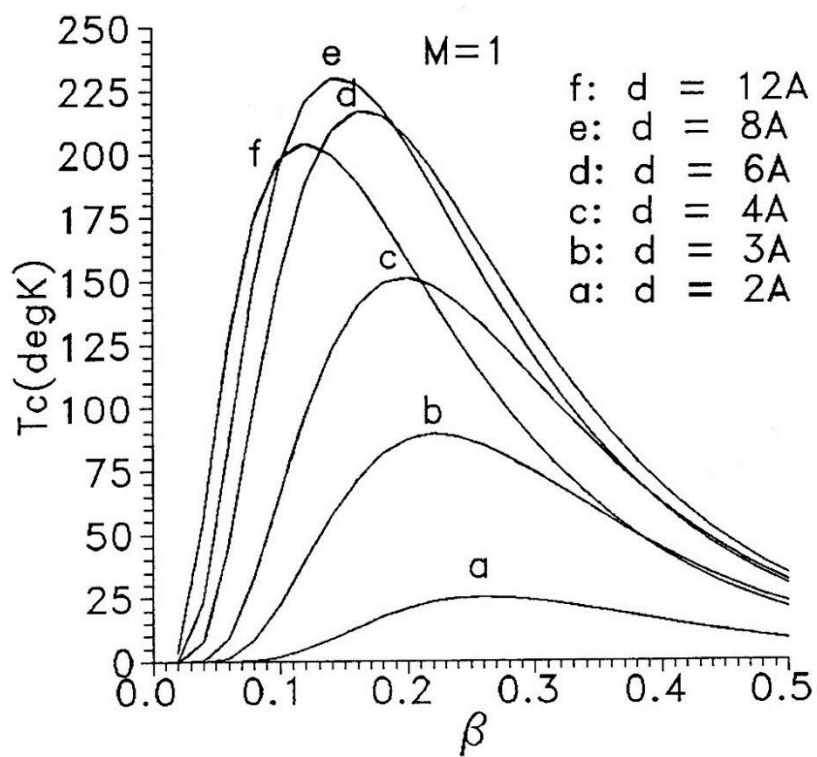


Fig. 6



(a)



(b)

Fig. 7

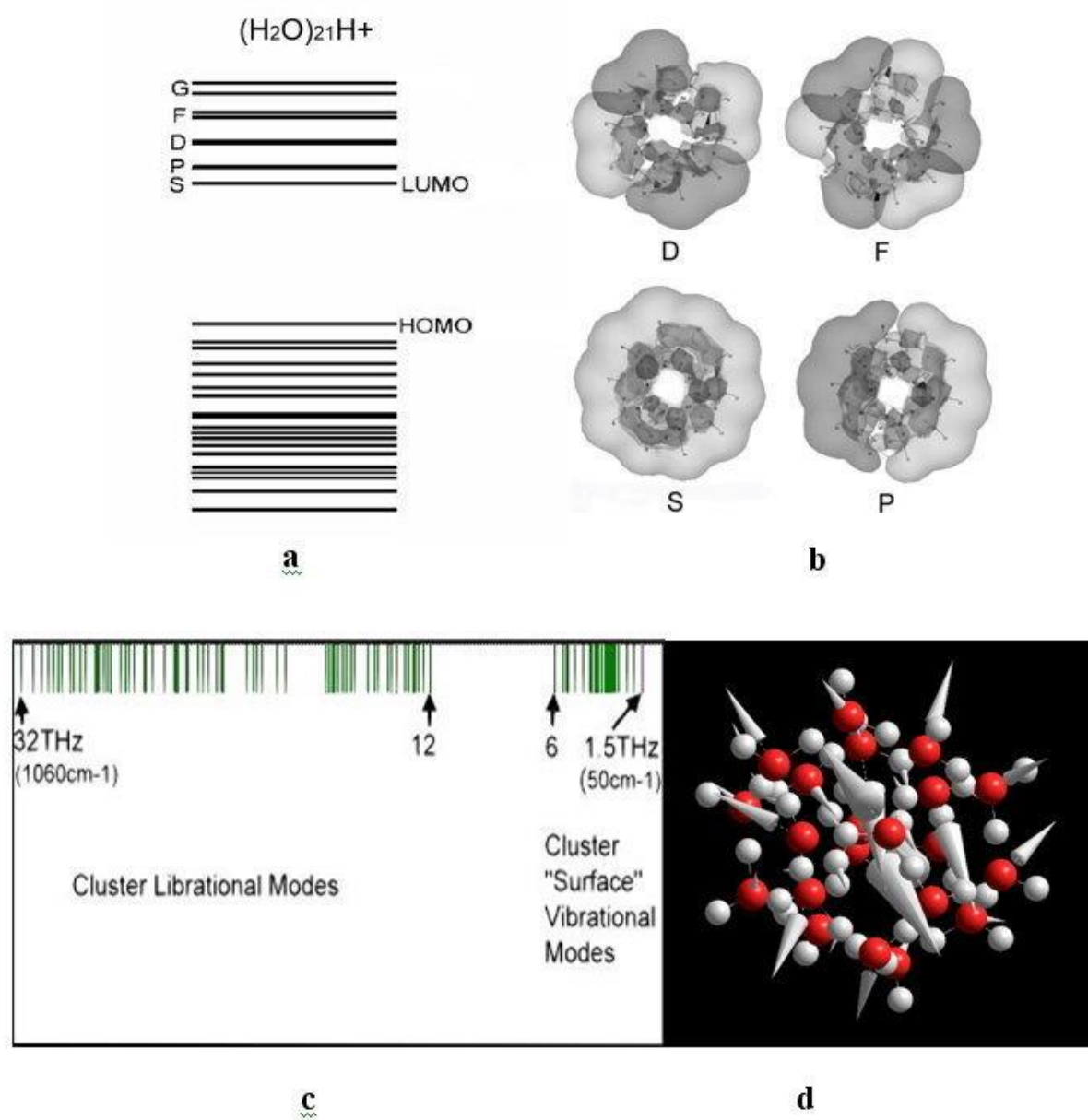


Fig. 8

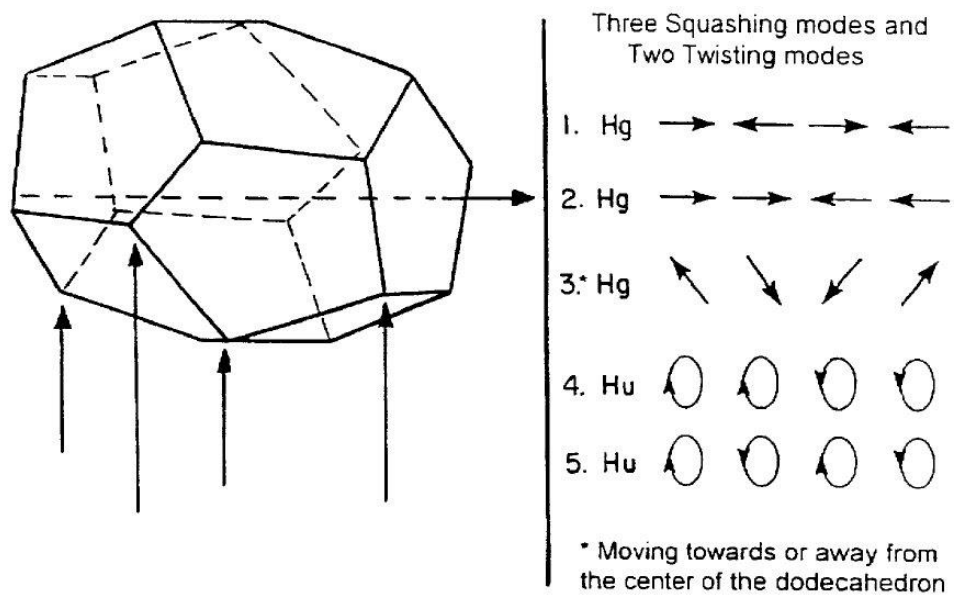


Fig. 9

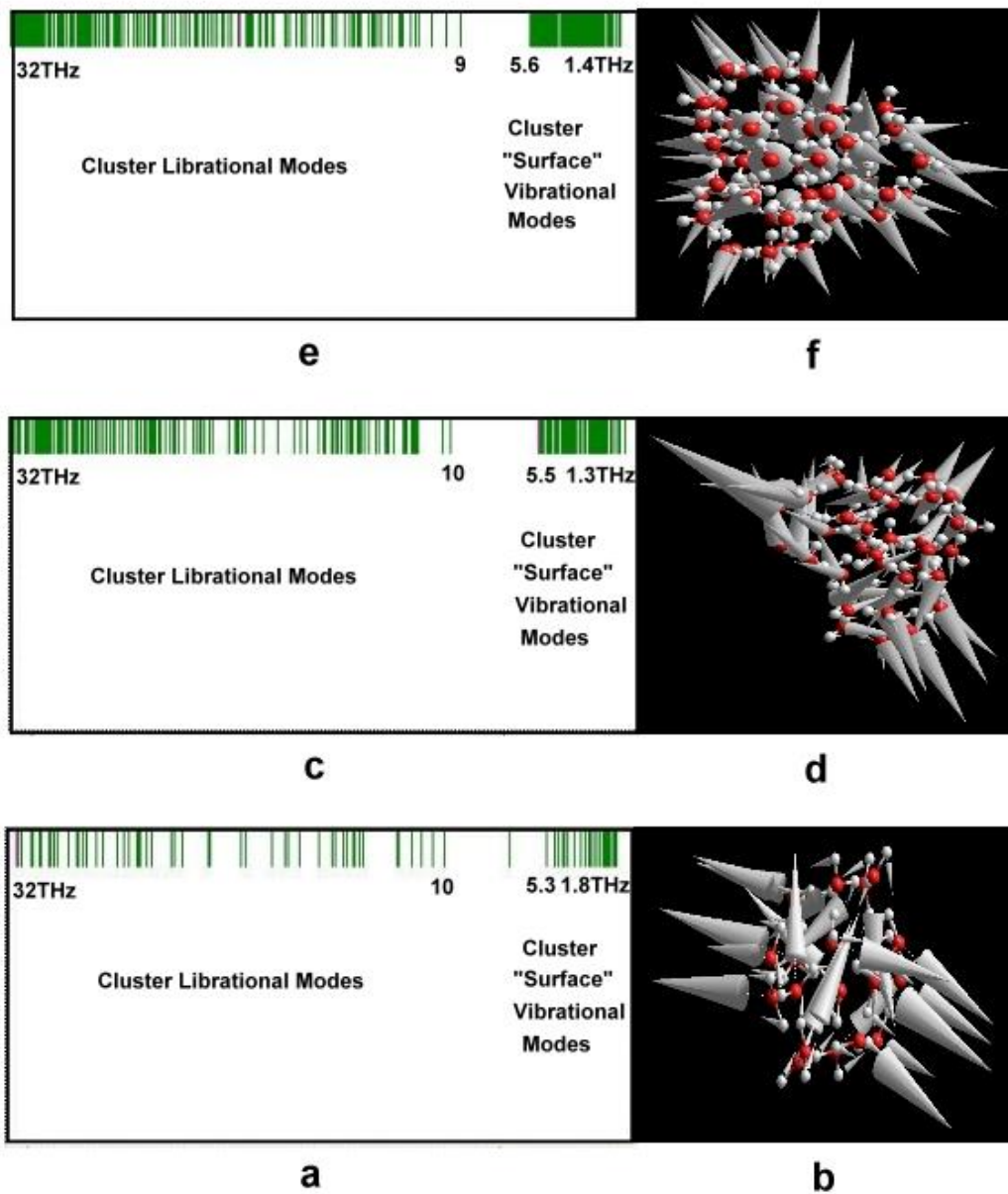
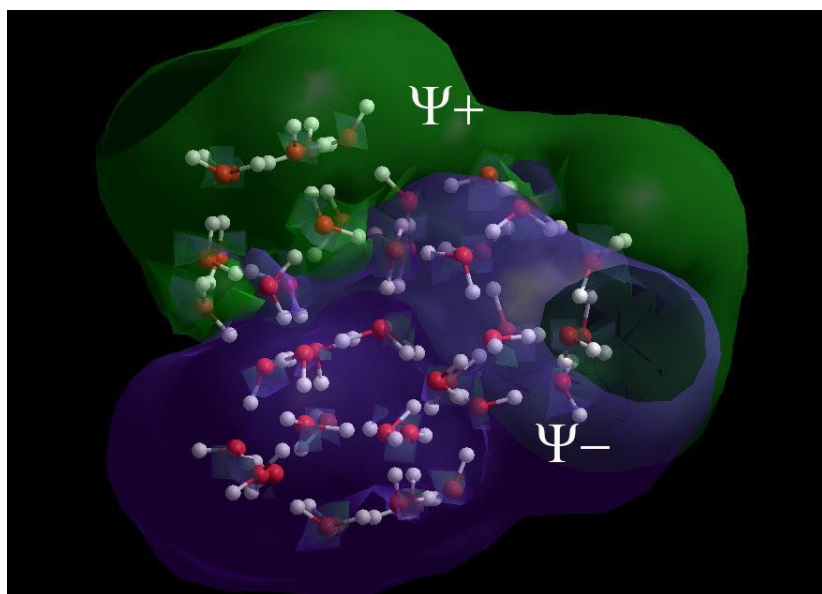
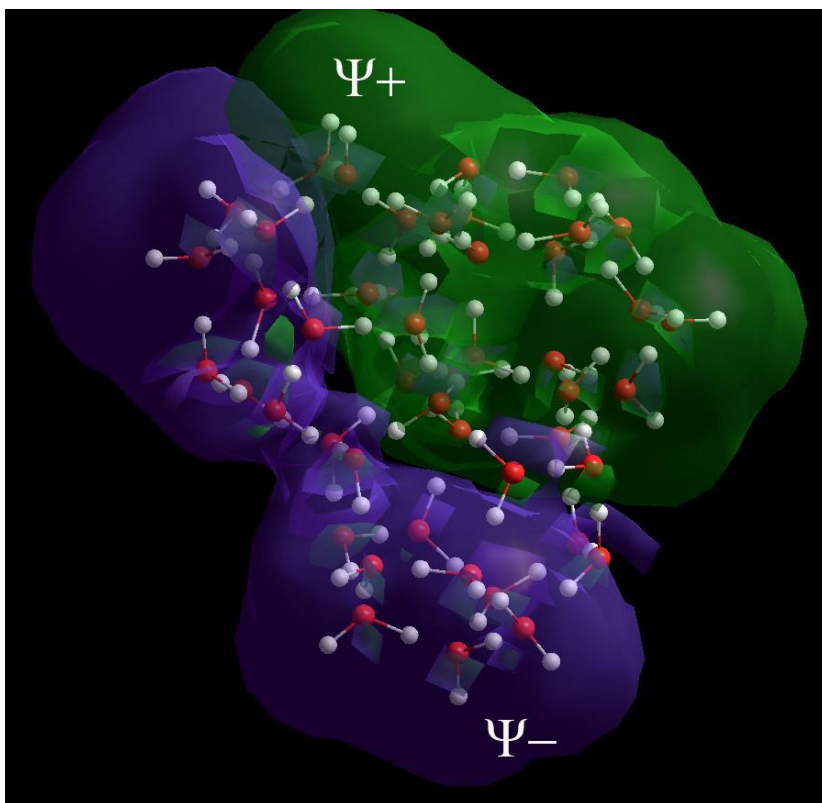


Fig. 10

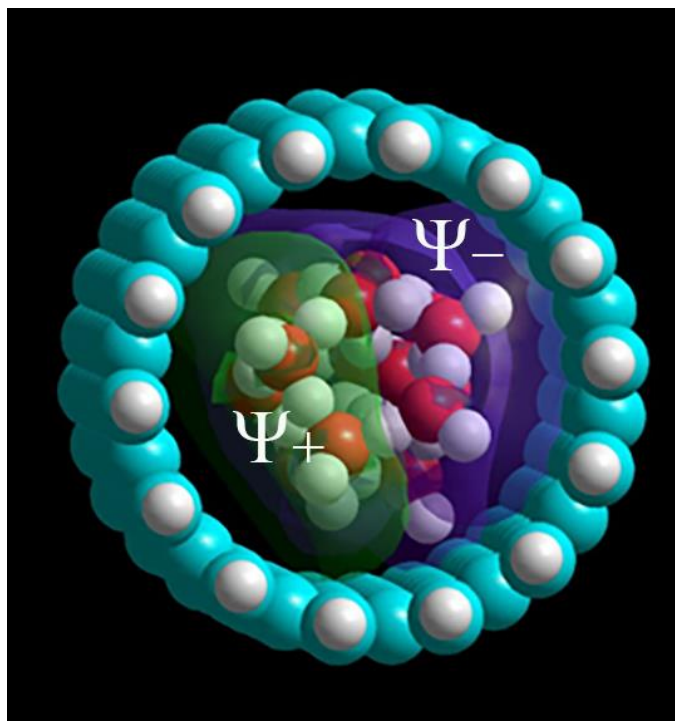


(a)

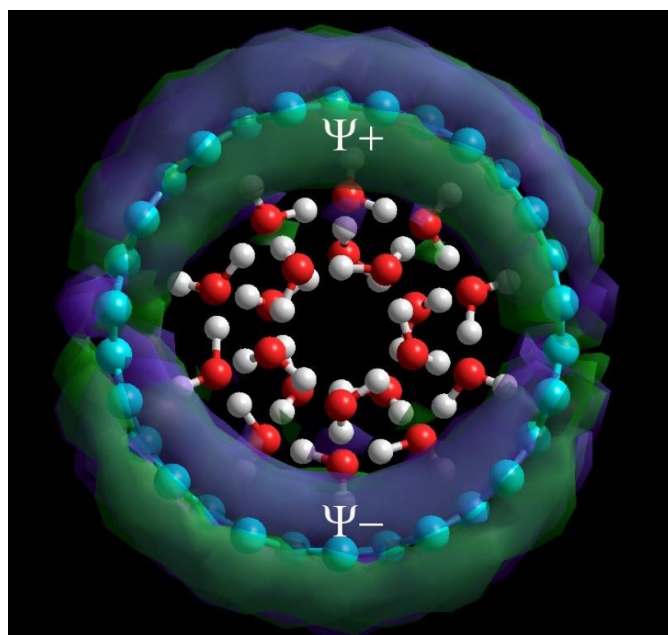


(b)

Fig. 11

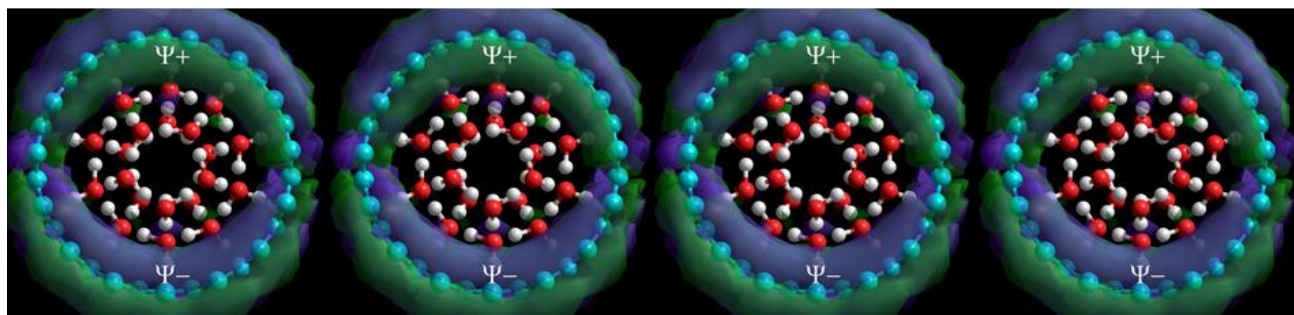


(a)

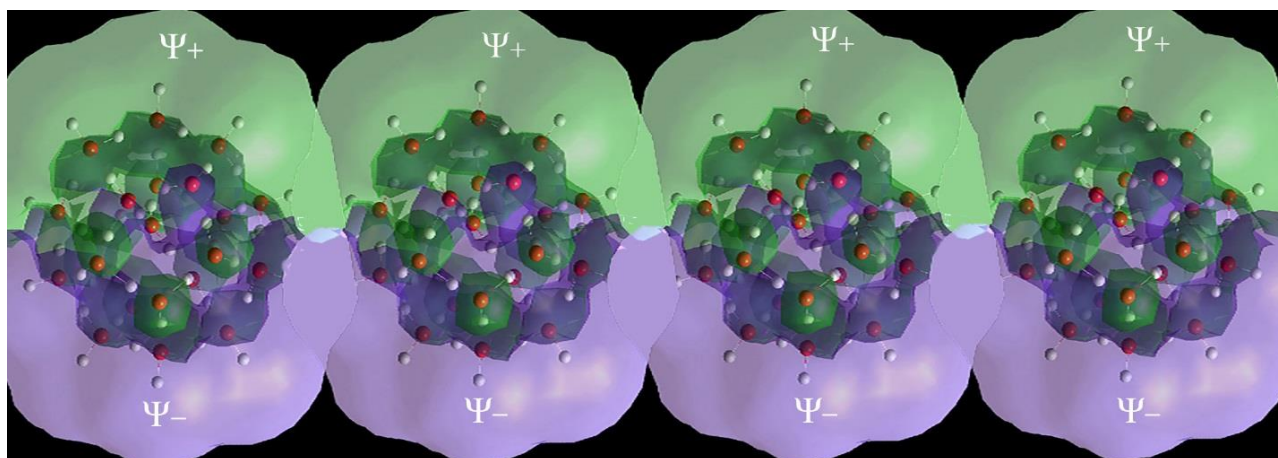


(b)

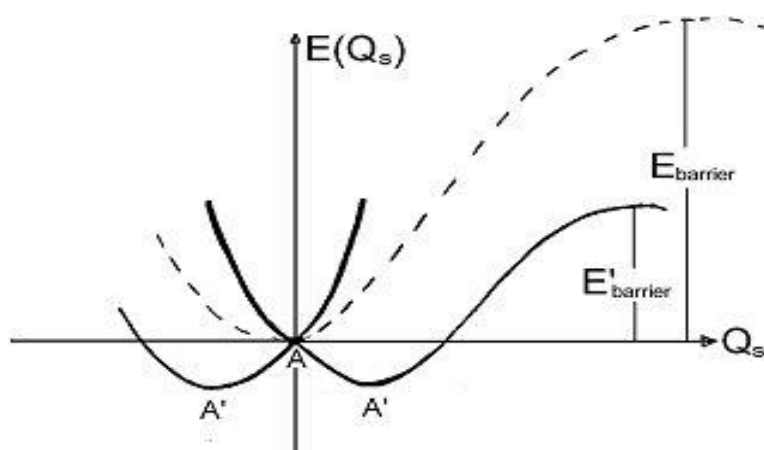
Fig. 12



(a)

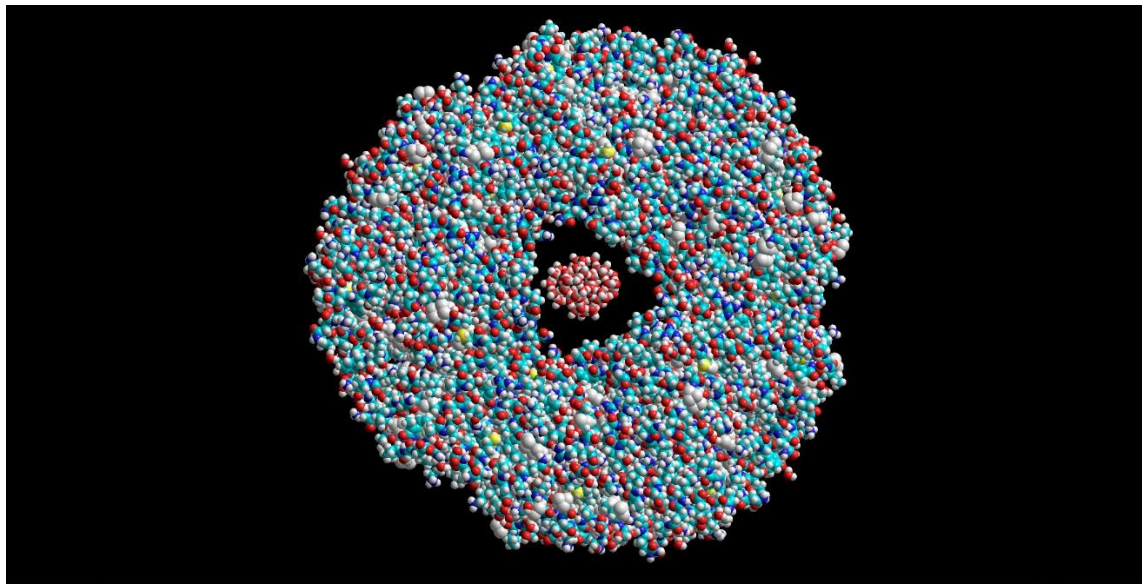


(b)

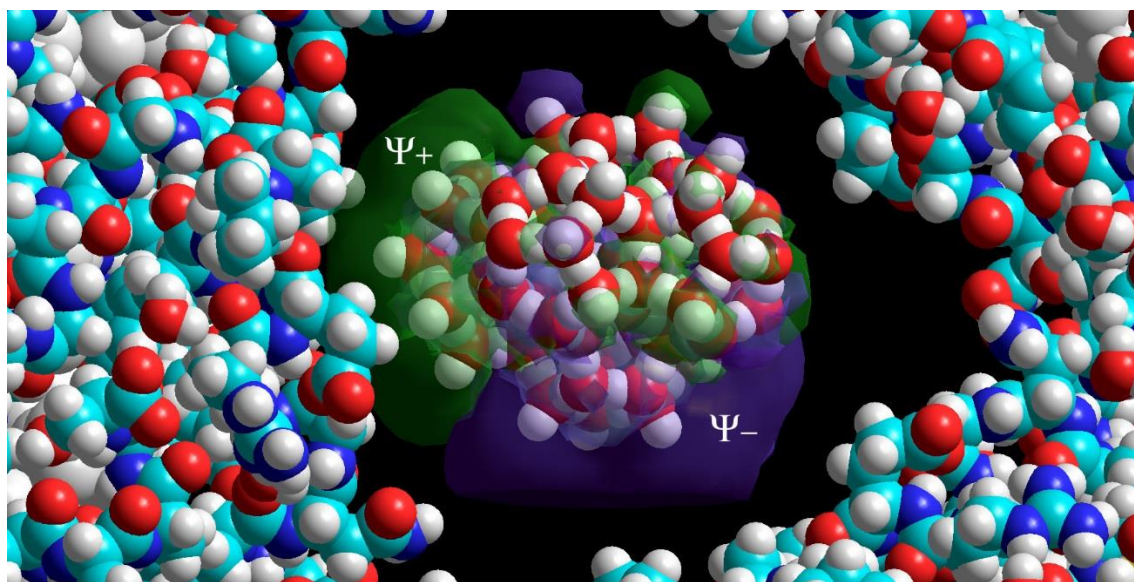


(c)

Fig. 13



(a)



(b)

Fig. 14